Supplementary Methods

Fibroblast Transcriptional Network Construction

Gene Regulatory Network Inference. We employed a previously published method of gene regulatory network inference to derive a network of transcription factor (TF)-target gene interactions based on a transcriptomic dataset of VIC populations after stimulation with patient sera. Bulk RNA-sequencing datasets recently published by our collaborators were used as a training set for network inference, and this dataset represents the gene expression of VIC populations stimulated with serum derived from a small cohort of patients undergoing a TAVR procedure(12). Briefly, patient blood samples were collected at the time of surgery and at the 1-month follow up visit (n = 4 female patient pairs and n = 8 male patient pairs, 24 samples total). Donors were 79.1±8.4 years of age on average, and all donors had a pre-TAVR aortic valve area <1.5 cm^2 (0.73±0.24 cm^2), suggesting an either moderate or severe stage of stenosis. The resulting serum samples were used to treat porcine VIC cultures seeded on soft PEG hydrogels (Young's modulus of 5.8 kPa) for 48 h prior to RNA-sequencing, and counts per million (CPM) for gene expression were used for subsequent network inference and model fitting methods. Of the total 24 samples collected, 16 samples were used for gene regulatory network inference and network parameter estimation (n = 4 female patient pairs and n = 4 male patient pairs), and 8 samples were retained for model validation only (n = 4 male patient pairs).

We utilized the GRNBoost2 machine learning algorithm to infer a network of TF-target interactions from the transcriptomic dataset above. This regression-based method is based on the GENIE3 tree-based algorithm for predicting regulatory links between input genes and target genes via the construction of decision tree ensembles(59). Each ensemble of decision trees, which predicts the expression of a given target gene from the expression of all input genes, is used to determine the relative "*importance*" of each input gene in predicting the expression of the specified target gene. Decision tree ensembles are built for all genes across the transcriptome, and input-target gene links are aggregated to form a composite network of ranked interactions. The GENIE3 algorithm has been shown to out-perform other methods in inferring gene regulatory networks as part of the DREAM4 *In Silico Multifactorial* challenge(60), and it provides several advantages over other common inference algorithms: (1) inference can be performed with minimal assumptions of network topology, (2) directed interactions (i.e. gene A activates gene B) can be inferred compared to correlation- and probability-based methods, and (3) non-linear or combinatorial regulation can be derived compared to other regression-based methods(61). The GRNBoost2 implementation optimizes this approach using stochastic gradient boosting, which grows decision tree ensembles on a subset of observations and estimates the loss function on the remaining observations with each iteration. The algorithm implements an early stopping criterion if the loss function does not improve above a set threshold, thereby preventing unnecessary iterations of each decision tree and reducing overall computational time(62). The Arboreto library for python was used to apply this algorithm to the RNA-sequencing data described above, and the average computational time for network inference using a 4-core computer was approximately 10 min.

Network Pruning. Upon inference of the initial network, a 3-step workflow was applied to filter the network for TF-target interactions that satisfy 3 requirements: (1) interactions must be supported by experimental evidence, (2) interactions must relate to either literature-supported TFs (primary TFs) or fibrosis-related target genes in myofibroblasts, and (3) resulting pathways connecting primary TFs and target genes must have relatively strong links across all individual edges as determined by interaction ranks assigned by the GRNBoost2 algorithm (Figure 1A). The first step was performed by comparing inferred TF-target interactions with databases of known TF-target interactions aggregated from chromatin immunoprecipitation (ChIP) studies. Curated lists of known TF-target interactions from the ChIP-X Enrichment Analysis (CHEA) and TRANSFAC databases were downloaded using the Harmonizome web interface(63), both of which were chosen to maximize coverage of TFs related to myofibroblast activation. Upon filtering the initial gene regulatory network for interactions contained in either database, the resulting network was filtered further for interactions containing TFs or fibrosis-related target genes in myofibroblasts. Lists of TFs and target genes were derived using our curated network model of myfibroblast signaling(64), which contains 11 primary TFs and 20 target genes coding for ECM-related proteins. For TFs that consist of several subunits (e.g. activator protein 1 [AP1] complex), both constituent genes were included for filtering. An additional 8 target genes that were differentially expressed by patients between pre- and post-TAVR sera were also considered: CTSC, CTSL, COL4A5, LOXL1, P4HA1, P4HA3, LAMA4, and ELN. Proteins coded by these genes have been shown to alter matrix degradation, collagen processing, and alter material properties of cardiac tissue, and significant differences in expression within the RNA-sequencing dataset provide a rationale for exploring possible regulatory pathways affecting gene expression. After list construction, the database-filtered network above was

filtered again for interactions containing genes in either list. After filtering, interactions contained only TF-TF interactions or TF-target interactions in which intermediate TFs not included in the primary TF list above regulate target gene expression (i.e. primary TF A activates secondary TF B, which activates target gene C).

After the second stage of filtering above, the final network topology was derived by ensuring that all resulting pathways between primary TFs and target genes contained interactions that ranked highly among possible regulatory links according to the GRNBoost2 algorithm. A modified depth-first-search algorithm was implemented to find all possible pathways between each primary TF and target gene and check whether each interaction within that pathway met this requirement using the "*importance*" score for the interaction output by GRNBoost2. Individual interactions were only allowed if the importance score of each edge was greater than either a threshold of 1 or the 75th percentile of all interactions stemming from the same TF. This hybrid threshold was chosen to both limit interactions driven by noise, in which overall importance scores are low, and to prevent premature exclusion of related interactions when all possible regulatory links may be ranked low relative to the entire network. By implementing this method, all interactions mediating expression of target genes were ensured to meet a threshold of confidence relative to neighboring interactions such that one TF within a pathway is not predictive of its downstream target. All network filtering steps were performed in a python environment using the numpy(65) and pandas(66) packages.

Composite Signaling/Transcriptional Network Implementation

Topological Integration. We combined the final transcriptional network with our previous myofibroblast signaling network describing intracellular mechanotransduction and chemotransduction(64) to form a composite network capable of predicting fibrosis-related protein expression in response to mechanical and biochemical stimuli. New TFs (model nodes) and/or transcriptional reactions (edges) were added to the cell signaling topology if they were not redundant to the original transcriptional reactions described by the signaling network.

Integration of Sex-Specific Signaling Pathways. To account for potential differences in signaling between male/female cell signaling during fibrosis, we incorporated a curated set of intracellular reactions encompassing estrogen transduction found via a manual literature search. Reactions were included if at least two independent studies contained experimental evidence in either VICs or cardiac myofibroblasts, resulting in an additional 7 nodes and 24 edges added to the network.

Logic-Based Ordinary Differential Equation Approach. The final network was implemented as a system of logic-based ordinary differential equations in which activity levels of all nodes were modeled by Hill equations. Logical NOT, AND, and OR gates were used for complex signaling interactions by applying the respective logical operations: $1 - f(x)$ for NOT gates, $f(x)f(y)$ for AND gates, and $f(x) + f(y) - f(x)f(y)$ for OR gates. The open-source Netflux package for MATLAB was used to build this system of differential equations(28), and all simulations were conducted using MATLAB (Mathworks, Natwick MA). All visualizations of network topology were constructed using Cytoscape(67).

Network Parameter Estimation

Dimensionality Reduction. To improve model predictions of myofibroblast behavior within the context of AVS before and after TAVR, we implemented a model fitting procedure to optimize the reaction weight parameters (w) of all reactions within the composite network. From the initial set of parameters (334 total), k-means clustering was conducted based on a global sensitivity analysis to group reaction weights based on changes in network-wide activity with knockdown. This method has been utilized in previous logic-based ordinary differential equation models to identify modules with similar functional behavior(17) and provides an advantageous method for reducing model dimensionality based on biological function. Reactions were clustered via the *kmeans* MATLAB function using k = 11, which was determined to produce the highest degree of separation between clusters. Reactions in which the product contained a fibrosis-related output gene were excluded from clustering to allow for additional degrees of freedom to predict the expression of individual output proteins, and k-means clustering was repeated 1000 times for the remaining reactions using randomly chosen starting points. Clusters of reactions occurring most frequently were assigned to final clusters and shared a weight parameter during fitting, thus reducing the dimensionality of the final parameter set for optimization (129 parameters total).

Multi-Omic Data Normalization. A genetic algorithm was used to fit the reduced parameter set above to normalized model input and output concentrations extracted from patient-specific proteomic and transcriptomic datasets recently published by our collaborators(12). In addition to the VIC RNA-sequencing data described above, relative concentrations of 1193 proteins from the same patient serum samples were measured via DNA

aptamer array, allowing for the direct relation of changes in serum proteins before and after TAVR to changes in myofibroblast activation. Using serum protein levels for all patients as input concentrations and VIC gene expression levels as output concentrations, data for each input and output node were transformed to a normalized scale useable by the model. All input levels were normalized between activity levels of 0.1 and 0.6 (representing 10% activation and 60% activation respectively), matching previous studies transforming biochemical cytokine and growth factor levels measured in myocardial tissue post-MI to normalized values while maximizing network dynamic range(68). All output levels were normalized between activity levels of 0.1 and 0.7, keeping the same basal values as input levels while expanding the dynamic range of output expression beyond the default half-maximal effective concentration (EC50) to account for multi-input stimulation. All normalized input levels were implemented as initial reaction weights within the model as representative rates of generation of each species, and all normalized output levels were implemented as steady-state concentrations of each species. Because not all input/output nodes were represented in the experimental datasets, unrepresented input reaction weights were included as parameters within the fitting parameter set, and unrepresented output activity levels were included for prediction but not used in the final objective function.

Global Parameter Estimation. Using normalized input/output sets for each patient, the *ga* MATLAB function was used for all parameter estimation. For each set of randomly generated parameter sets within the function, steady-state output levels for each patient were measured after 80 h given either pre-TAVR or post-TAVR levels for that patient. Changes in steady-state output levels were calculated for each patient from pre-TAVR levels to post-TAVR levels ($\Delta Activity_{TAVR}$), and the mean squared error (MSE) between $\Delta Activity_{TAVR}$ values and experimental changes in normalized gene expression between conditions ($\Delta Expression_{TAVR}$) for all patients and outputs were used as the objective function. An population size of 500 and 100 subsequent generations were chosen to maximize intra-generational variation while limiting computational resources. Program defaults were used for all other algorithm hyperparameters, and default values for the cell signaling model were used for all other model parameters including Hill coefficient (n), EC50, maximum node activation (Y_{max}), and time constant (τ) (69). Due to the stochastic nature of generating initial parameter sets for global optimization, the model fitting procedure was repeated 50 times using random initial parameter sets resulting in an ensemble of parameter sets. Predicted node activity levels for all subsequent simulations reflect the mean activity levels predicted across all estimated parameter sets.

Network Perturbation Analysis

To identify influential signaling mechanisms across pre-TAVR and post-TAVR signaling contexts, a series of node knockdowns were simulated using normalized input levels from each patient serum sample. For each set of normalized input levels used during parameter estimation above, basal conditions (i.e. without any knockdown) were applied for 80 h, followed by knockdown of individual nodes using the Y_{max} parameter ($Y_{max,KD} = 0.1*Y_{max,basal}$) for 240 h. Steady-state activity levels of all nodes were measured with each knockdown, and changes in node activity ($\Delta Activity_{KD}$) were calculated as the difference between node activity after knockdown and basal node activity. Knockdown sensitivity of each node was calculated as the sum of absolute $\Delta Activity_{KD}$ levels for the node across all knockdown simulations, and knockdown influence of each node was calculated as the sum of absolute $\Delta Activity_{KD}$ levels for all other nodes in the network upon knockdown.

Patient stratification analysis

Targeted simulations assessing stratified model responses to drug targets with patient-specific conditions were conducted using a series of dose-response simulations. For each node, a series of knockdown simulations was performed under each patient-specific condition. Following a simulation of basal conditions using each patient's normalized input levels for 80 h, the Y_{max} parameter for each node was lowered to either 0.8, 0.6, 0.4, or 0.2 times the Y_{max} under basal conditions for 240 h (corresponding with 20-80% node inhibition). Steady-state activity levels of all nodes were measured with each dose and compared to steady-state levels prior to dosing. Patients were then classified as 'responder' or 'non-responder' based on a simple over-under threshold, which was varied from 0 to the maximum delta for each protein output to generate receiver-operating-characteristic curves.

In vitro validation experiments

PEG Hydrogel Fabrication. Poly(ethylene glycol) (PEG) hydrogels were made as previously described(12). 25 mm glass coverslips were O_2 plasma-treated and treated in a 15% vol/vol

mercaptopropyltrimethoxysilane (MPTS, Sigma-Aldrich) and 5% vol/vol 2-butylamine (Sigma-Aldrich) solution in toluene (Sigma-Aldrich) for 2 hours to functionalize the glass with free thiols. Coverslips were rinsed with toluene, dried in a 80°C oven, and sterilized with 70% ethanol. Gel precursor solutions (4% wt/vol PEG-norbornene [Nb]) were prepared by mixing 8-arm 40 kDa PEG-Nb with 5 kDa PEG-dithiol crosslinker (JenKem) and 2 mM CRGDS cell adhesive peptide (Bachem) at a 0.99:1 thiol-to-ene ratio in phosphate buffered saline (PBS, Sigma-Aldrich). Lithium phenyl-2,4,6-trimethylbenzoylphosphinate (LAP, 1.7 mM) was added to the pre-cursor solution prior to photo-polymerization. The gel pre-cursor solution was sandwiched between a coverslip and a Sigmacote (Sigma) treated microscope glass slide (final gel thickness = 150 μm for 25 mm coverslips), UV-photopolymerized at 4 mW/cm^2 for 3 minutes, sterilized in 5% isopropyl alcohol in PBS for 30 minutes, washed 3 times with PBS, and swelled overnight in VIC media at 37°C and 5% CO_2.

VIC isolation and culture. Male or female porcine valvular interstitial cells (VICs) were harvested from porcine aortic valve leaflets as previously described(12, 70). Briefly, aortic valve leaflets were excised from fresh porcine hearts from 5-6-month-old young adult pigs (Hormel), rinsed in warmed Earle's Balanced Salt Solution (EBSS, Sigma-Aldrich) supplemented with 50 U/mL penicillin (Thermo Fisher), 50 μg/mL streptomycin (Thermo Fisher), and 1 μg/mL amphotericin B (Thermo Fisher). Leaflets were transferred to a 250 units type II collagenase (Worthington) per mL EBSS solution and incubated at 37°C and 5% CO_2 for 30 minutes under constant shaking. Leaflets were vortexed at maximum speed for 30 seconds, transferred to fresh collagenase solution, and incubated at 37°C and 5% CO_2 for 60 minutes under constant shaking. Leaflets were vortexed again for 2 minutes at maximum speed and cells were passed through a 100 μm cell strainer using sterile transfer pipettes. Cells were centrifuged at 0.2*g* for 10 minutes, and pellets were resuspended in VIC expansion medium consisting of Media 199 (Life Technologies), 15% fetal bovine serum (FBS, Life Technologies), 50 U/mL penicillin, 50 μg/mL streptomycin, and 1 μg/mL amphotericin B. Cells were cultured at 37°C and 5% CO_2 on tissue culture treated polystyrene (TCPS) for expansion before experiments. 70-80% confluent VIC cultures were harvested using trypsin (Life Technologies) and counted using an automated hemocytometer. VICs were seeded on PEG hydrogels at a density of 20,000 cells per cm^2 growth area in Media 199 supplemented with 1% serum (FBS or human serum samples), 50 U/mL penicillin, 50 μg/mL streptomycin, and 1 μg/mL amphotericin B. In order to consider sex-specific VIC gene expression, VICs were sex-matched to each human serum sample such that female sera were applied to female VICs and vice versa.

RT-PCR. RNA was extracted from male or female aortic valvular interstitial cells in culture using a RNeasy Micro Kit (Qiagen) according to the manufacturer's protocol. RNA quality was assessed via spectrophotometry (ND-1000, NanoDrop), and cDNA was synthesized using an iScript Synthesis kit (Bio-Rad) according to the manufacturer's protocol. Relative mRNA expression was determined using SYBR Green reagents on an iCycler (Bio-Rad). Normalizations were performed using the *RPL30* gene. Primer sequences are provided in **Table 1**.

Table 1: Primer sequences

Gene	Forward Primer (5'-3')	Reverse Primer (5'-3')
RPL30	AGATTTCCTCAAGGCTGGGC	GCTGGGGTACAAGCAGACTC
MMP9	CATTCAAGGAGACGCCCACT	GCCTTTTGCGTTTCCGAAGT
COL1A1	GGGCAAGACAGTGATTGAATACA	GGATGGAGGGAGTTTACAGGAA
TIMP1	GCGGATACTTCCACAGGTCC	TCCAGGGAGCCACAAAACTG
SPP1	GCGTCTTCTGAGATCAACTG	CACATATACATTCACCAACTAAGC
SERPINE1	CCAAAGGGCGCTGAATAGTA	TGCTTTCCAAATTCCAAAAACT

Statistical analyses

Computational model data are shown as mean levels across the ensemble of model parameter sets. Significant differences between pre-TAVR and post-TAVR groups were determined using two-tailed Student's t-tests in MATLAB. Correlations between activity data were determined using Pearson correlation in MATLAB, and Student's t-tests with Benjamini-Hochberg correction for multiple comparisons were used to assess statistical significance. An aggregated matrix content score (MCS) was also derived for each patient from individual output activity levels using rank-normalized values. Model outputs were rank-normalized for each patient, and mean activity levels for all procollagens and matricellular proteins ($Activity_{Matrix}$), mean activity levels for all matrix proteases ($Activity_{Protease}$), and mean activity levels for all protease inhibitors were used for

aggregation: $MCS = Activity_{Matrix} - Activity_{Protease} + Activity_{Inhib}$. Output nodes were categorized as follows: $Activity_{Matrix}$: proCI, proCIII, fibronectin, periostin, osteopontin, LOXL1, P4H; $Activity_{Protease}$: proMMPs 1, 2, 3, 8, 9, 12, 14, CTSC, CTSL; $Activity_{Inhib}$: TIMP1, TIMP2, PAI1. Correlations involving MCS levels were determined using Spearman correlation in MATLAB and Student's t-tests for statistical significance.

In vitro experimental mRNA measurements were analyzed using a one-way ANOVA with post-hoc Sidak's post-hoc tests to directly compare bosentan treated vs. untreated groups in each patient-specific serum context. Six replicates were measured for each condition.

Supplementary Figures

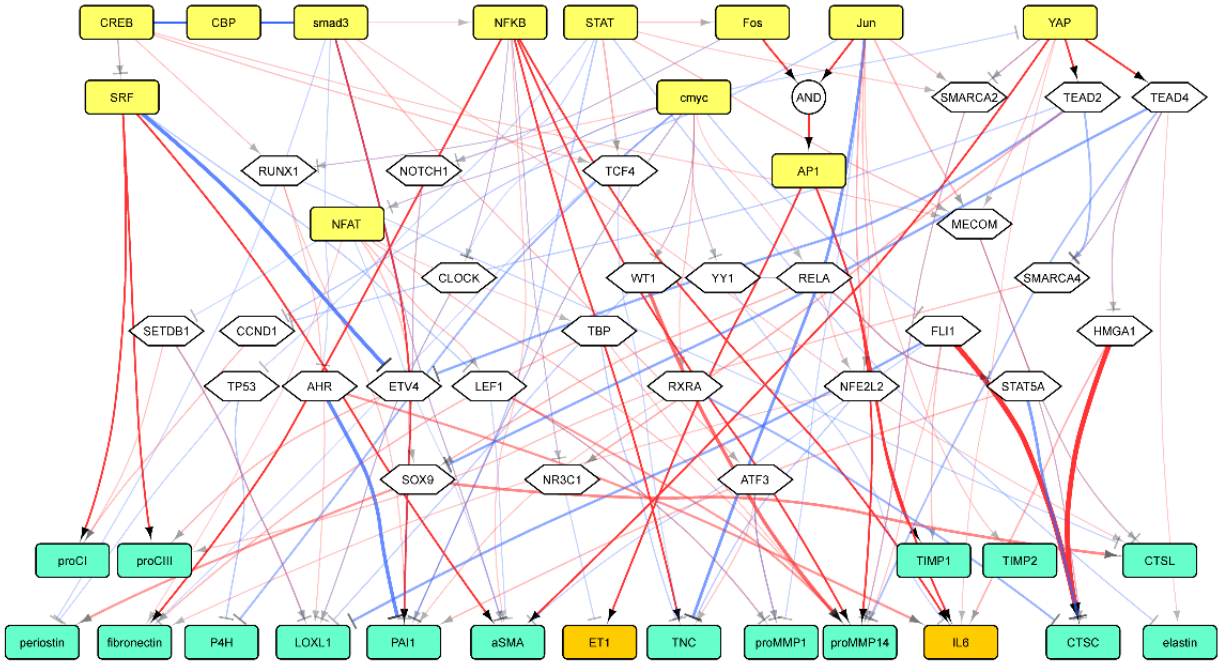

Figure S1. Schematic of inferred transcriptional network. Signaling-activated TFs (yellow boxes), secondary TFs (white hexagons), and model outputs associated with fibrosis or autocrine feedback (green/orange boxes) are connected by directed activation and inhibition reactions (red and blue arrows, respectively). Edge widths and transparency represent relative "importance" scores of each TF-target interaction as measured via the GRNBoost2 algorithm.

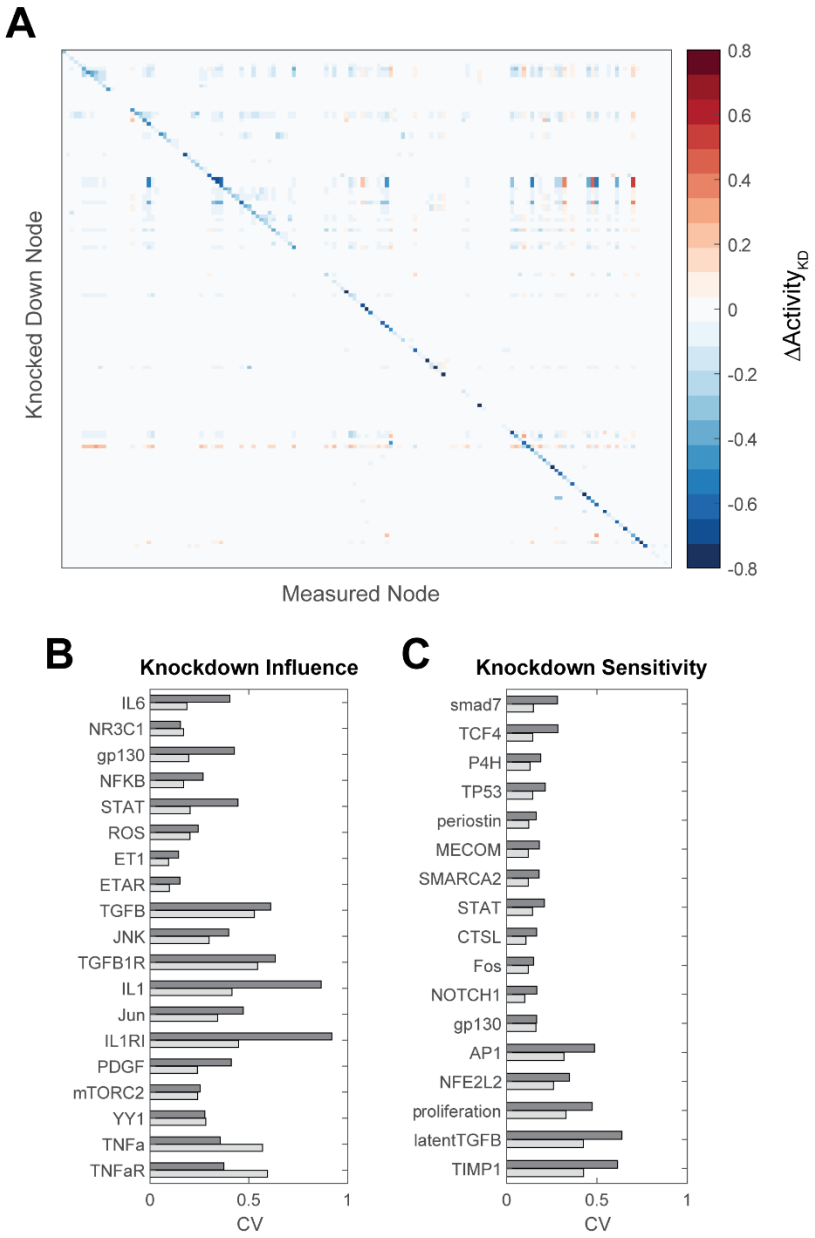

Figure S2. Full network perturbation analysis results. (A) Changes in activity for all nodes in the network were measured following comprehensive knockdown of individual nodes (Ymax = 0.1) under individual patient pre- and post-TAVR conditions. Values reflect average changes in node activity between perturbed and un-perturbed conditions with each patient condition. Refer to the model logic file available on GitHub for the order of nodes perturbed/measured. (B/C) Coefficients of variation (CV) across patient cohort for node influence and sensitivity values. Dark bars represent CVs for each pre-TAVR patient condition, and light bars represent values for each post-TAVR patient condition.